ABSTRACT

Finite-Element Ray Tracing

by
Yong-chun Liu

The interesting acoustic modeling problems often push the practical limits of full-wave models. For instance, in acoustic tomography one needs to be able to predict the propagation of an acoustic pulse for successive realizations of 3D environments. For these types of problems ray methods continue to be attractive because of their speed. Unfortunately, existing codes are prone to a number of implementation difficulties which often degrade their accuracy.

As a result most ray models are actually incapable of producing the ray theoretic result. We discuss a new method for implementing ray theory that uses a finite-element formulation. This method is free of artifacts affecting standard ray models and provides excellent agreement with more computationally intensive full-wave models.

FINITE-ELEMENT RAY TRACING

by
Yong-chun Liu

A Thesis
Submitted to the Faculty of
New Jersey Institute of Technology
in Partial Fulfillment of the Requirements for the Degree of
Master of Science in Applied Mathematics

Department of Mathematics

October 1993

APPROVAL PAGE

Finite-Element Ray Tracing

Yong-chun Liu

Dr. Michael B. Porter, Thesis Adviser — Date
Associate Professor of Applied Mathematics, NJIT

Dr. Ellen Livingston, Committee Member — Date
Research Mathematician, Acoustic Division, Naval Research Laboratory, Washington DC

Dr. Gregory Kriegsmann, Committee Member — Date
Chairperson and Professor of Applied Mathematics, NJIT

BIOGRAPHICAL SKETCH

Author: Yong-chun Liu

Degree: Master of Science in Applied Mathematics

Date: August, 1993

Undergraduate and Graduate Educations:

- Master of Science in Applied Mathematics,
  New Jersey Institute of Technology, Newark, NJ, 1993
- Master of Engineering in Electrical Engineering,
  Zhejiang University, Hangzhou, China, 1990
- Bachelor of Applied Mathematics,
  Zhejiang University, Hangzhou, China, 1987

Major: Applied Mathematics

ACKNOWLEDGMENT

I wish to express my sincere gratitude to my supervisor, Dr. Michael B. Porter, for his guidance, friendship and moral support throughout my graduate study. He also helps me a lot on non-academic affairs. My thanks to him are beyond my words.

Also, I would like to express my special thanks to Professors Livingston and Kriegsmann for serving as members of committee. Professor Livingston pointed out many mistakes in the thesis.

I appreciate the timely help and suggestions from Mr. Haitao Jiang.

TABLE OF CONTENTS

Chapter **Page**

CHAPTER 1

INTRODUCTION AND DERIVATION OF RAY THEORY

1.1 Introduction to Ray Theory

Ray-based models were very popular many years ago in underwater acoustics. Today, however ray tracing codes have fallen somewhat out of favor in this research community. A recent survey [9] of available navy models concluded that none of the tested models was satisfactory for transmission loss model. The main reason ray models have languished is that improvements in computer performance have made full-wave solutions practical. These full-wave approaches are not subject to the accuracy limitations caused by the high-frequency approximation in ray methods.

Two common problems occur in ray theory predictions [7]:

- *shadow zones* where no rays pass and therefore the acoustic pressure is identically zero in this zone.
- *caustics* which are curves where the cross-section of a ray tube vanishes and therefore the predicted intensity is infinite.

Nevertheless, ray theory retains some key advantages. The ray paths themselves provide a clear indicator of the paths along which energy propagates. This information is much harder to extract from full-wave models. Furthermore, broad-band problems have become increasingly important and ray models are especially efficient for such problems. For instance, acoustic tomography relies on time-of-flight information to image the ocean. Ray models have been used almost exclusively to provide this sort of broad-band prediction.

The goal of this thesis is to develop an improved numerical approach to ray model. The method, which we refer to as *finite element ray tracing* combines ideas from Gaussian beam tracing [13] and the finite element method. Like Gaussian beam

tracing, the resulting algorithm is particularly simple to implement. The primary difference is that 'hat'-shaped basis functions are used instead of Gaussian functions. This seemingly small difference leads to significant differences in the nature of the solution. The Gaussian functions are in many ways a natural basis of the wave equation. The equations governing the spreading and wave-front curvature for the beams are derived from a paraxial solution of the wave equation. In contrast, the finite element beams are chosen for purely numerical reasons. They lead to a piecewise linear approximation of the acoustic field.

Thus, the resulting algorithm combines features of ray and beam models. Most importantly, the appealing structural simplicity of a Gaussian beam code is preserved. However, unlike Gaussian beam tracing the initial beamwidth and curvature are precisely defined. Picking good values for these parameters remains one of the key difficulties of Gaussian beam codes. The trade-off is that finite-element ray tracing does retain the problems of caustics and shadow zones that are intrinsic to ray tracing. In the following sections we will review the underlying equations of ray tracing. Our derivation follows Ref. [7] closely.

1.2 Derivation of Ray Theory

The fundamental equation of acoustics is the wave equation. The wave equation can be derived from the mass-continuity equation and Euler momentum equations. Two important approximations are required. One is that the flow can be treated as *inviscid*. The other is that *convective derivatives* are negligible compared to unsteady derivatives. Further details are provided in Ref. [16].

In an ideal fluid, the wave equation can be written as:

$$\nabla^2 p(\mathbf{x}, t) - \frac{1}{c^2(\mathbf{x}, t)} \frac{\partial^2 p(\mathbf{x}, t)}{\partial t^2} = 0, \tag{1}$$

where p is the pressure field, c is the sound speed as a function of time t and space $\mathbf{x}$.

When sources are introduced, the wave equation can be expressed in a general inhomogeneous form:

$$\nabla^2 p(\mathbf{x},t) - \frac{1}{c^2(\mathbf{x},t)}\frac{\partial^2 p(\mathbf{x},t)}{\partial t^2} = f(\mathbf{x},t), \tag{2}$$

where $f(\mathbf{x},t)$ is a volume force.

Since the time scale of oceanographic change is much longer than the time scale of acoustic propagation, we can assume the sound speed is independent of time, i.e.

$$c(\mathbf{x},t) = c(\mathbf{x}). \tag{3}$$

Using the frequency-time Fourier transform pairs

$$f(t) = \frac{1}{2\pi}\int_{-\infty}^{\infty} F(\omega)e^{-i\omega t}d\omega, \tag{4}$$

$$F(\omega) = \int_{-\infty}^{\infty} f(t)e^{i\omega t}dt, \tag{5}$$

we can then write Eq. (2) as:

$$\nabla^2 p(\omega,\mathbf{x}) + \frac{\omega^2}{c^2(\mathbf{x})}p(\omega,\mathbf{x}) = F(\omega,\mathbf{x}). \tag{6}$$

This is called the Helmholtz or reduced wave equation.

In the case of a monochromatic (single frequency) point source the inhomogeneous term assumes the form of a delta function so that we obtain:

$$\nabla^2 p(\mathbf{x}) + \frac{\omega^2}{c^2(\mathbf{x})}p(\mathbf{x}) = -\delta(\mathbf{x}-\mathbf{x}_\mathrm{s}), \tag{7}$$

where ω is the circular frequency of the source which is located at $\mathbf{x}_s$.

To solve the Helmholtz equation, we seek a solution in the form of a *ray series*.

$$p(\mathbf{x}) = e^{i\omega\tau(\mathbf{x})}\sum_{j=0}^{\infty}\frac{A_j(\mathbf{x})}{(i\omega)^j}. \tag{8}$$

Here τ is the phase of the pressure and $A_j(\mathbf{x})$ is the amplitude of the pressure.

Taking derivatives of p(x) with respect to its component x, we obtain p_x and p_{xx} respectively:

$$p_x = e^{i\omega\tau}\left(i\omega\tau_x\sum_{j=0}^{\infty}\frac{A_j}{(i\omega)^j} + \sum_{j=0}^{\infty}\frac{A_{j,x}}{(i\omega)^j}\right), \tag{9}$$

$$p_{xx} = e^{i\omega\tau}\left(\left[-\omega\tau_x^2 + i\omega\tau_{xx}\right]\sum_{j=0}^{\infty}\frac{A_j}{(i\omega)^j} + 2i\omega\tau_x\sum_{j=0}^{\infty}\frac{A_{j,x}}{(i\omega)^j} + \sum_{j=0}^{\infty}\frac{A_{j,xx}}{(i\omega)^j}\right). \quad (10)$$

Thus we can write

$$\nabla^2 p = e^{i\omega\tau}\left(\left[-\omega|\nabla\tau|^2 + i\omega\nabla^2\tau\right]\sum_{j=0}^{\infty}\frac{A_j}{(i\omega)^j} + 2i\omega\nabla\tau\cdot\sum_{j=0}^{\infty}\frac{\nabla A_j}{(i\omega)^j} + \sum_{j=0}^{\infty}\frac{\nabla^2 A_j}{(i\omega)^j}\right). \quad (11)$$

Substituting this result into the Eq. (7) and equating terms of like order in ω, the following equations for $\tau(\mathbf{x})$ and $A_j(\mathbf{x})$ are obtained:

$$O(\omega^2): \qquad |\nabla\tau|^2 = \frac{1}{c^2(\mathbf{x})}, \quad (12)$$

$$O(\omega): \qquad 2\nabla\tau\cdot\nabla A_0 + (\nabla^2\tau)A_0 = 0, \quad (13)$$

$$O(\omega^{1-j}): \qquad 2\nabla\tau\cdot\nabla A_j + (\nabla^2\tau)A_j = -\nabla^2 A_{j-1}, \quad j = 1, 2, \ldots \quad (14)$$

Equation (12) for $\tau(\mathbf{x})$ is known as the eikonal equation while the equations for $A_j(\mathbf{x})$ are called the *transport* equations.

We retain only the lowest order transport equation. This is obviously a high frequency approximation. Next we will show how to solve the eikonal equation and transport equation.

1.2.1 Solving the Eikonal Equation

Note that, the eikonal equation is a nonlinear equation. To solve the eikonal equation we introduce auxiliary variables and perform some manipulations to reduce this nonlinear equation to the familiar form involving first order ordinary differential equations (ODEs).

The first step is to introduce a family of curves (rays) that are perpendicular to the wave-fronts (curves where the phase of the wave $\tau(\mathbf{x})$ is a constant). This is illustrated in the Fig. 1.

This family of curves defines a new coordinate system, ray coordinates. In these coordinates, the eikonal equation can be reduced to a much simpler system of ODEs.

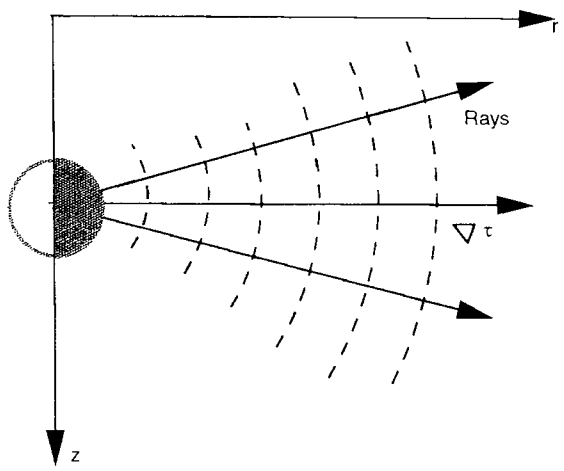

Figure 1: Rays and wave-front (from Ref. [7])

The ray trajectory $\mathbf{x}(s)$ satisfies the following differential equation:

$$\frac{d\mathbf{x}}{ds} = c\nabla\tau, \tag{15}$$

where s denotes arclength along the ray and the factor c was included so that the tangent vector of $d\mathbf{x}/ds$ has unit length. We now consider the particular case of cylindrical coordinates. Then the trajectory of the ray in the range-depth plane is represented as $(r(s), z(s))$. In these coordinates, we obtain the following equations from Eq. (15):

$$\begin{aligned} \frac{dr}{ds} &= c\frac{\partial\tau}{\partial r}, \\ \frac{dz}{ds} &= c\frac{\partial\tau}{\partial z}. \end{aligned} \tag{16}$$

Note that the phase $\tau(\mathbf{x})$ is still unknown. However, with some manipulations we can write the ray equations in a form involving only $c(\mathbf{x})$.

To reduce the nonlinear eikonal equation, we introduce some auxiliary variables ρ and ζ, which are proportional to the local tangent vector of ray trajectory. These equations may be written in the first-order form:

$$\begin{aligned} \frac{dr}{ds} &= c\rho(s), \\ \frac{dz}{ds} &= c\zeta(s). \end{aligned} \tag{17}$$

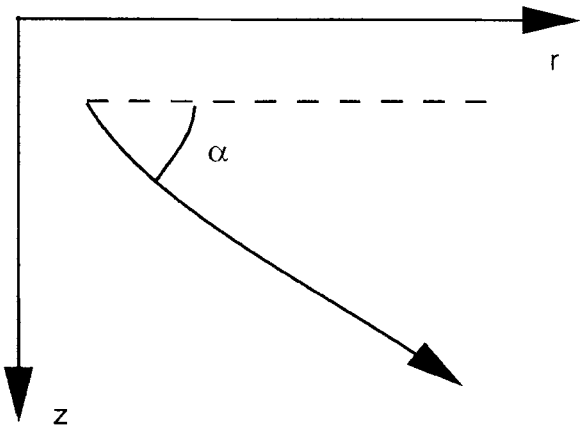

Figure 2: Schematic of ray geometric and take-off angle

Using Eq. (17), Eq. (16) and Eq. (12), we calculate

$$\begin{aligned}
\frac{d\rho}{ds} &= \frac{d}{ds}\left(\frac{1}{c}\frac{dr}{ds}\right) = \frac{d}{ds}\left(\frac{\partial\tau}{\partial r}\right) \\
&= \frac{\partial^2\tau}{\partial r^2}\frac{dr}{ds} + \frac{\partial^2\tau}{\partial r\partial z}\frac{dz}{ds} \\
&= c\left(\frac{\partial^2\tau}{\partial r^2}\frac{\partial\tau}{\partial r} + \frac{\partial^2\tau}{\partial r\partial z}\frac{\partial\tau}{\partial z}\right) \\
&= \frac{c}{2}\frac{\partial}{\partial r}\left[\left(\frac{\partial\tau}{\partial r}\right)^2 + \left(\frac{\partial\tau}{\partial z}\right)^2\right] \\
&= \frac{c}{2}\frac{\partial}{\partial r}\left(\frac{1}{c^2}\right) = -\frac{1}{c^2}\frac{\partial c}{\partial r}.
\end{aligned} \tag{18}$$

Similarly, we obtain an equation for ζ:

$$\frac{d\zeta}{ds} = -\frac{1}{c^2}\frac{\partial c}{\partial z}. \tag{19}$$

Putting this all together, we obtain the ray equations in the first-order form:

$$\begin{aligned}
\frac{dr}{ds} &= c\rho(s), \\
\frac{dz}{ds} &= c\zeta(s), \\
\frac{d\rho}{ds} &= -\frac{1}{c^2}\frac{\partial c}{\partial r}, \\
\frac{d\zeta}{ds} &= -\frac{1}{c^2}\frac{\partial c}{\partial z}.
\end{aligned} \tag{20}$$

In this form, the ray equations can be solved using standard numerical integrators (Euler's Method or Runge-Kutta) for systems of ODEs. However, we shall first need initial conditions. Each ray starts from the source with a take-off angle α, as shown in Fig. 2. Thus, we have the initial conditions as follows:

$$\begin{aligned} r(0) &= r_s, \\ z(0) &= z_s, \\ \rho(0) &= \frac{\cos\alpha}{c(0)}, \\ \zeta(0) &= \frac{\sin\alpha}{c(0)}. \end{aligned} \tag{21}$$

The source position is obviously a known quantity. The take-off angle α is determined by which ray we choose to calculate.

Calculating $r(s)$, $z(s)$, $\rho(s)$ and $\zeta(s)$ is, however, only an intermediate step. Our purpose is to obtain the pressure field. The pressure field is determined by two components, the pressure amplitude and the its phase. In ray coordinates, it is easy to calculate the phase τ. We rewrite Eq. (12) as:

$$\nabla\tau \cdot \nabla\tau = \frac{1}{c^2}. \tag{22}$$

Using Eq. (15), this reduces to

$$\nabla\tau \cdot \frac{1}{c}\frac{d\mathbf{x}}{ds} = \frac{1}{c^2}, \tag{23}$$

or,

$$\frac{d\tau}{ds} = \frac{1}{c}. \tag{24}$$

This is the eikonal equation written in terms of the ray coordinate s. Solving this differential equation, we obtain:

$$\tau(s) = \tau(0) + \int_0^s \frac{1}{c(s')} ds'. \tag{25}$$

The integral term in this equation is the travel time along the ray, so that this equation is simply stating that the phase of the ray is delayed according to travel time.

1.2.2 Solving the Transport Equation

Let us recall the transport equation:

$$2\nabla\tau \cdot \nabla A_0 + (\nabla^2\tau)A_0 = 0, \tag{26}$$

Substituting Eq. (15) into the above equation, we get

$$\frac{2}{c}\frac{d\mathbf{x}}{ds} \cdot \nabla A_0 + (\nabla^2\tau)A_0 = 0. \tag{27}$$

This can be rewritten,

$$\frac{2}{c}\frac{dA_0}{ds} + (\nabla^2\tau)A_0 = 0. \tag{28}$$

To solve Eq. (28), we use the following property [7] of the Jacobian determinant (denoted by J)

$$\nabla^2\tau = \frac{1}{J}\frac{d}{ds}\left(\frac{J}{c}\right), \tag{29}$$

Thus Eq. (13) can be written as:

$$2\frac{dA_0}{ds} + \left[\frac{c}{J}\frac{d}{ds}\left(\frac{J}{c}\right)\right]A_0 = 0. \tag{30}$$

Integrating this equation, we obtain the final result for the solution of the transport equation:

$$A_0(s) = A_0(0)\left|\frac{c(s)J(0)}{c(o)J(s)}\right|^{1/2}. \tag{31}$$

To complete the solution of the transport equation we must have formulas for the Jacobian determinant and the initial amplitude. In general three dimensional coordinates, the Jacobian determinant can be expressed as:

$$J = \left|\frac{\partial\mathbf{x}}{\partial(s,\alpha,\beta)}\right|, \tag{32}$$

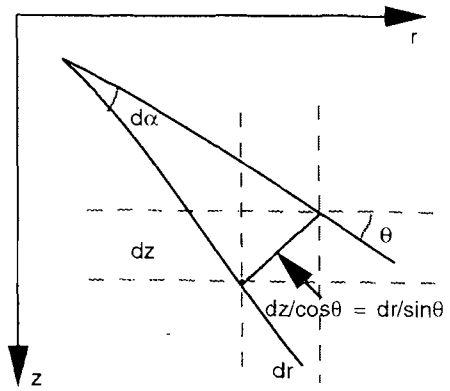

Figure 3: The ray tube cross-section

where α and β are respectively the declination and azimuthal take-off angles of the ray. In our cylindrically symmetric problem, this can be written:

$$J = r\left(\frac{\partial r}{\partial s}\frac{\partial z}{\partial \alpha} - \frac{\partial z}{\partial s}\frac{\partial r}{\partial \alpha}\right), \tag{33}$$

or,

$$J = r\left[\left(\frac{\partial z}{\partial \alpha}\right)^2 - \left(\frac{\partial r}{\partial \alpha}\right)^2\right]^{1/2}. \tag{34}$$

As shown in Fig. 3, the Jacobian determinant can be written as:

$$J = \frac{r}{\cos\theta}\frac{\partial z}{\partial \alpha}, \tag{35}$$

and,

$$J = \frac{r}{\sin\theta}\frac{\partial r}{\partial \alpha}, \tag{36}$$

where θ is the angle of the ray at the receiver.

To find the initial values we use the 'method of canonical problems'. Consider a point source in an infinite homogeneous medium. We know the solution of this problem:

$$p^0(s) = \frac{e^{i\omega s/c_0}}{4\pi s}, \tag{37}$$

where s is the distance from the source to the receiver. The amplitude and phase associated with this solution are:

$$A^0(s) = \frac{1}{4\pi s}, \tag{38}$$

$$\tau^0(s) = \frac{s}{c_0}. \tag{39}$$

Note that $\tau(0) = 0$, however, as $s \to 0$, $A_0 \to \infty$.

In this homogeneous case, the rays are straight lines fanning out from the source. The ray equations can be easily solved:

$$\mathbf{x}(s) = \mathbf{x}_s + s(\cos\alpha\cos\beta, \cos\alpha\sin\beta, \sin\alpha). \tag{40}$$

From these ray paths the Jacobian determinant is calculated as:

$$J(s) = -s^2\cos\alpha. \tag{41}$$

We note that:

$$\lim_{s\to 0} A_0(s)|J(s)|^{\frac{1}{2}} = \frac{1}{4\pi}|\cos\alpha|^{\frac{1}{2}}. \tag{42}$$

is a bounded value. So Eq. (31) can be written as:

$$A_0(s) = \frac{1}{4\pi}\left|\frac{c(s)\cos\alpha}{c(o)J(s)}\right|^{1/2}. \tag{43}$$

Combining Eq. (25) and Eq. (43), we write the pressure field as:

$$p(s) = \frac{1}{4\pi}\left|\frac{c(s)\cos\alpha}{c(o)J(s)}\right|^{1/2} e^{i\omega\int_0^s \frac{1}{c(s')}ds'}. \tag{44}$$

In the next chapter we will discuss the numerical solution of these equations.

CHAPTER 2

FINITE ELEMENT RAY TRACING

2.1 Finite Element Ray Tracing

In the last chapter we provided the governing equations to calculate the pressure field along each ray. In the study of underwater acoustics we are concerned with the pressure field at any point. Sometimes it is difficult to find the eigenray that connects the source and a particular receiver point. Furthermore, as we discussed in Chap. 1, there are some blemishes of the standard ray tracing method. So several informal attempts have been put forward to improve the ray tracing results to achieve an answer which more closely resembles reality. One popular approach is Gaussian beam tracing [13, 3].

The construction of Gaussian beams begins with the central ray which satisfies the usual ray equations. Then one constructs beams about the rays by integrating a pair of auxiliary equations, which govern the evolution of beam in terms of the beam width and the curvature as a function of arc length. The resulting pressure field describes a beam whose amplitude decays in a Gaussian fashion as a function of normal distance from the central ray of the beam.

Encouraged by the idea of Gaussian beams, we introduce finite element rays (FER) in which a triangular beam is constructed as shown in Fig. 4. Whether or not a ray contributes at a particular receiver point depends on the normal distance from the ray to the receiver. Beyond the width of the triangle defining the beam there is no contribution to the field.

Note that the amplitude along a ray depends on the change in area of the ray tube. There exist simple differential equations that provide information about how the ray paths change for infinitesimal perturbations in either the ray take-off angles or the

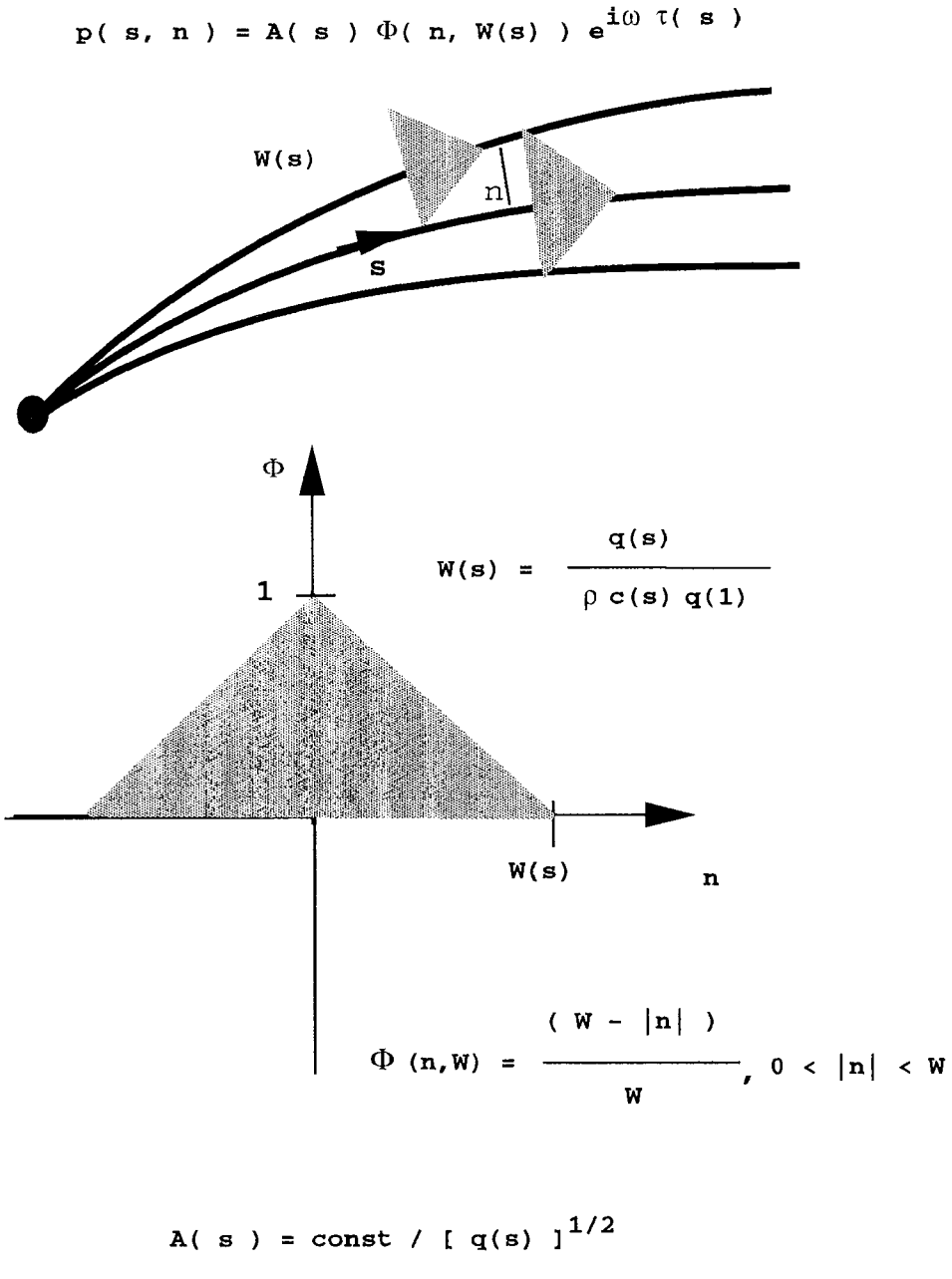

Figure 4: Construction of a finite-element ray.

ray source point. These are the so-called *dynamic ray equations*:

$$\begin{aligned} \frac{dq}{ds} &= cp(s), \\ \frac{dp}{ds} &= -\frac{c_{nn}}{c^2(s)}q(s), \end{aligned} \tag{45}$$

where c_{nn} is the derivative of the sound speed in a normal direction to the ray path. Written in terms of depth and range derivatives:

$$c_{nn} = c^2(c_{rr}\zeta^2 - 2c_{rz}\zeta\rho + c_{zz}\rho^2). \tag{46}$$

The type of the perturbation is determined by the initial conditions. If we take

$$q(0) = 0, \qquad p(0) = \frac{1}{c(0)}, \tag{47}$$

then we are perturbating the rays with respect to angle. It turns out that we can then relate the Jacobian and the q function by the relation (Ref. [7]):

$$rq(s) = J(s). \tag{48}$$

We can write the ray amplitude as

$$A_0(s) = \frac{1}{4\pi}\left|\frac{c(s)\cos\alpha}{r\,c(o)q(s)}\right|^{1/2}. \tag{49}$$

The quantities $p(s)$ and $q(s)$ are easily obtained by integrating the dynamic ray equations along the central ray.

We use the width of the central ray to determine whether the ray contributes to the receiver or not. There are three steps to calculate the width of tube:

- From Eq. (43), we know

$$J(s) = \left|\frac{1}{4\pi A_0(s)}\right|^2 \frac{c(s)\cos\alpha}{c(0)\,r}. \tag{50}$$

- δz can be approximated by the Jacobian determinant

$$\begin{aligned} \delta z &= \frac{\delta\alpha\, J(s)}{r}\cos\theta \\ &= \frac{\delta\alpha\, J(s)\, c\,\rho}{r}. \end{aligned} \tag{51}$$

- The beam width $W(s)$ is therefore related to δz via

$$\begin{aligned} W(s) &= \frac{\delta z}{\cos^2\theta} = \frac{\delta\alpha\, J(s)\, c\,\rho}{r\,\cos^2\theta} \\ &= \frac{\delta\alpha\, r\, q\, c\,\rho}{r\,\cos^2\theta} = \left|\frac{q\,\delta\alpha}{c\,\rho}\right|, \end{aligned} \tag{52}$$

where $\delta\alpha$ is the difference in angles between adjacent rays.

The contribution of each ray within the ray tube is then determined by:

$$p'(s) = \frac{W(s) - n(s)}{W(s)} p(s), \tag{53}$$

where $n(s)$ is the normal distance from the receiver to the contributing ray.

2.2 Boundary Reflections

So far we have discussed the finite element rays without considering bottom and surface reflections. In deep water, the field is often dominated by purely refracted paths and we may ignore the reflected rays. However, in shallow water, typically all rays are bottom reflected. Thus, the reflected rays play a very important role in the wave propagation. We will now show how to calculate such rays in our finite element formulation.

Whenever the ray strikes the sea floor or surface, it splits into two parts as shown in Fig. 5: one is reflected, the other is transmitted. Thus, part of the energy is absorbed by the bottom and the pressure amplitude of the reflected ray declines. The amplitude of the reflected ray is determined by a reflection coefficient which depends on the ray angle θ and medium properties.

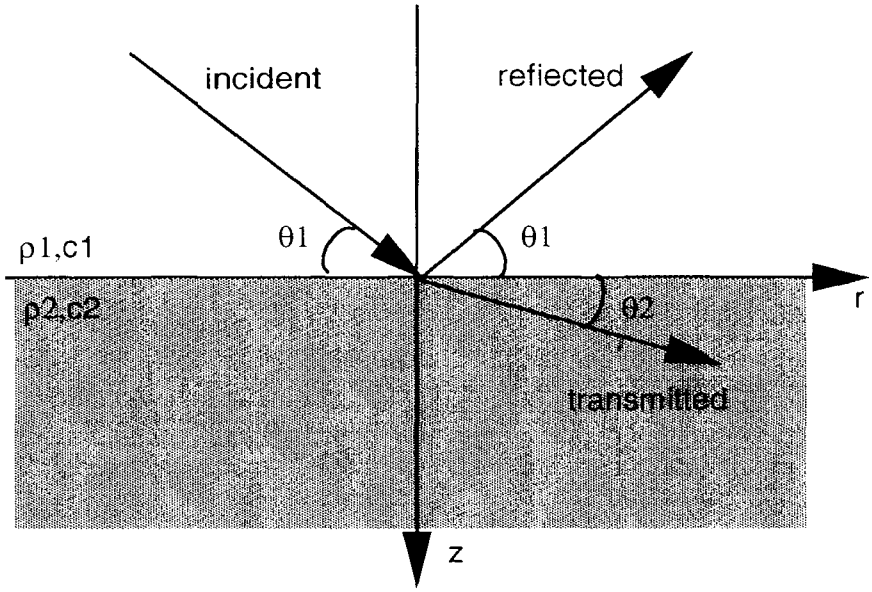

Figure 5: Reflection and transmission at different interfaces

We consider three types of boundary conditions which are determined by the characteristics of the materials: rigid, vacuum, and half-space.

For the vacuum boundary, the reflection coefficient is

$$R(\theta) = e^{i\pi}. \tag{54}$$

Since the magnitude of R is one we have perfect reflection. However, the non-zero argument indicates that there is a phase change.

For the rigid boundary, the reflection coefficient is

$$R(\theta) = 1. \tag{55}$$

The ray is completely reflected as in the vacuum boundary case, but the phase of the reflected ray is unchanged.

The half-space boundary is the most interesting case. As mentioned above, when the ray strikes the boundary it splits into two rays: a reflected ray and a transmitted ray. The phase and amplitude associated with each ray is determined by the complex reflection coefficient. Since we are not interested in the field in the half-space we can

neglect the transmitted ray and focus our attention on the reflected ray.

The reflection coefficient $R(\theta)$ at the bottom is given by

$$R(\theta) = \frac{\rho_2\gamma_1 - i\rho_1\gamma_2}{\rho_2\gamma_1 + i\rho_1\gamma_2}. \tag{56}$$

Here, ρ is the density, c is the sound speed and γ is the vertical wave-number. The subscripts 1 and 2 refer to the upper and lower media respectively. Furthermore, γ_1, γ_2 are vertical wave-numbers defined by:

$$\begin{aligned} \gamma_1 &= (\omega^2/c_1^2 - k^2)^{1/2}, \\ \gamma_2 &= (k^2 - \omega^2/c_2^2)^{1/2}. \end{aligned} \tag{57}$$

Here k is the horizontal wave-number which is related to the angle of incidence θ via:

$$k = \omega\ c\cos\theta, \tag{58}$$

where ω is the circular frequency of the wave. Note, that the reflection coefficient is a complex number so there is an effect on both the magnitude and phase of the reflected ray.

To incorporate these effects in the FER formulation we simply carry along an extra function to keep track of the boundary losses. This function is set to unity at the start of the ray trace and decremented in accordance with the reflection loss after each boundary interaction. The phase change on reflection is incorporated directly into the phase function $\tau(s)$.

CHAPTER 3

NUMERICAL EXAMPLES

In this chapter we present a few examples to demonstrate the performance of the finite element ray (FER) method. The examples are chosen to include typical ocean acoustic problems in the Pacific and Arctic and including both shallow and deep water. Solutions obtained using the FER approach will be compared to reference solutions obtained using either the fast field program (FFP) or a normal mode solution[7]. The particular FFP and normal mode models used are SCOOTER and KRAKEN [14]

3.1 Isovelocity Case

The isovelocity case is the most simple and intuitive case. Since the sound speed is constant, the ray propagates as a straight line and the transmission loss follows a simple spherical spreading law. Figure 6 shows the ray trace with the anticipated straight line paths. The source is at the depth of 50 m where the depth of the bottom is 100 m. We present only a few rays with take-off angles in $[-14^o, 14^o]$.

The ray plot also shows reflections off the surface and bottom of the waveguide. Of course, the amplitude associated with these rays is determined by the reflection coefficient. We shall consider different cases involving vacuum and half-space boundary conditions. When the half-space parameters are chosen to be the same as those of the ocean medium, the reflected ray has vanishing amplitude and therefore makes no contribution to the pressure field.

In the first case, we use homogeneous half-spaces for both the surface and bottom boundaries. As a result we suppress any reflected waves. The resulting transmission loss obtained using the FER and FFP models is shown in Fig. 7. Here the source is located at 50 m with a frequency of 250 Hz. The plot shows a smooth decay in amplitude reflecting the spherical energy decay of a homogeneous medium. The agreement of the two models is excellent. A more precise indicator of the agreement

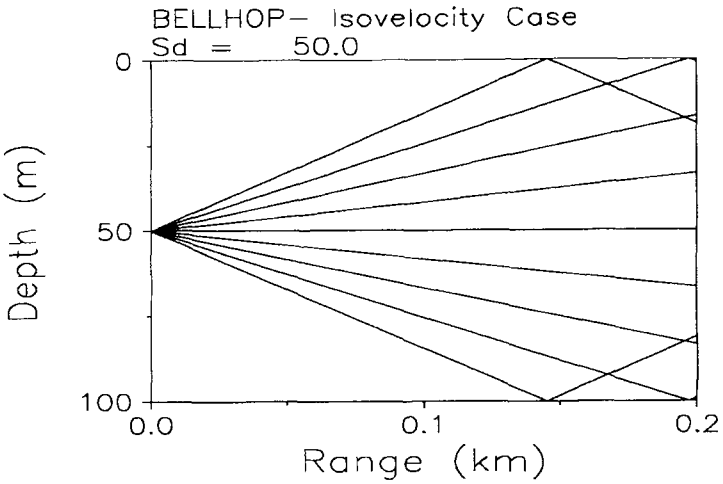

Figure 6: Ray trace for the isovelocity case.

may be seen by taking a slice through this field. This is displayed in Fig. 8 for a receiver depth of 80 m. The FER and FFP results are plotted using a dashed and solid line respectively. The agreement is so good that it is not possible to distinguish the two curves. This is to be expected in a properly functioning model since ray theory is exact for a homogeneous medium.

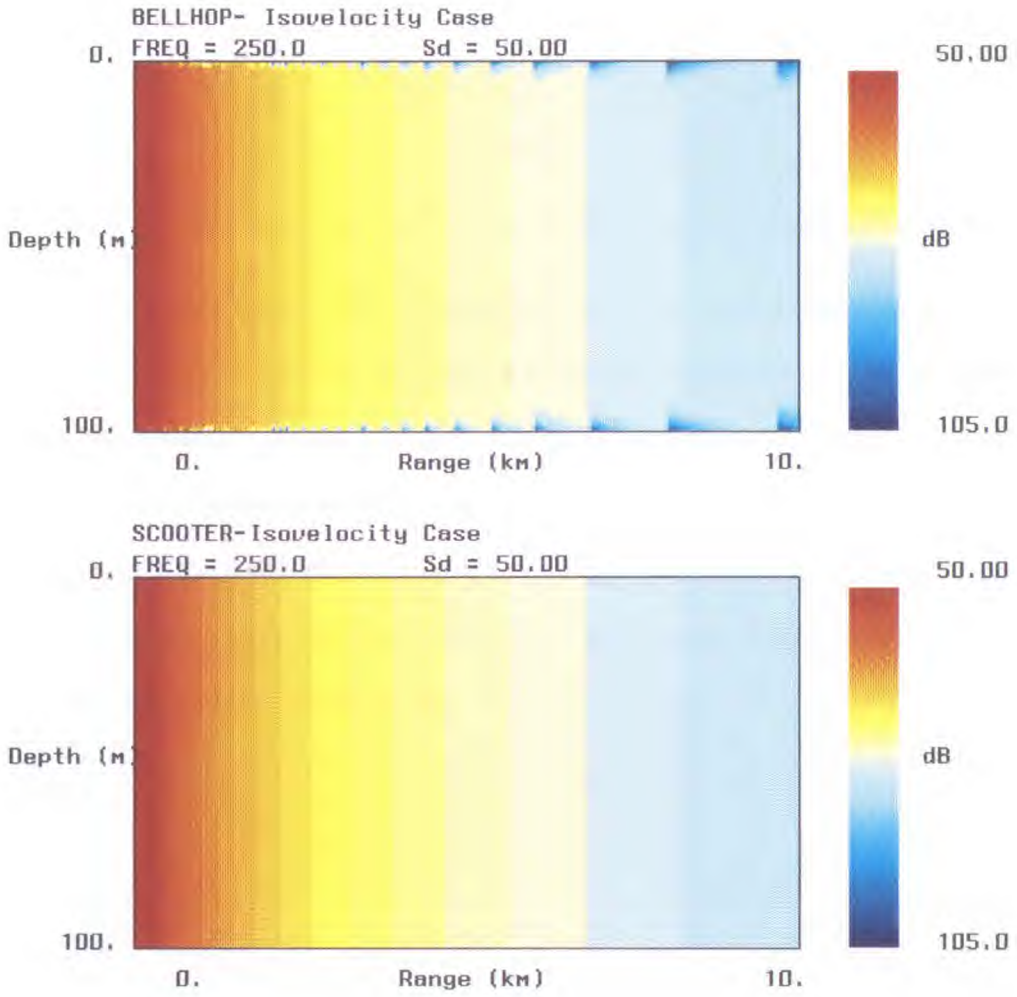

Figure 7: Transmission loss for the isovelocity case with half-space boundaries.

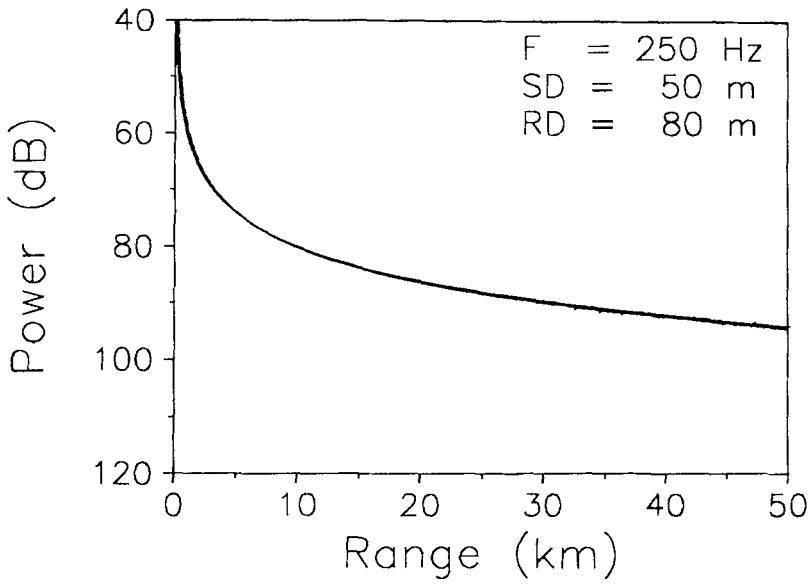

Figure 8: Transmission loss for the isovelocity case with half-space boundaries.

In the next case we modify the previous problem by introducing a vacuum at the ocean surface. As a result we obtain a strong out-of-phase surface reflection. The resulting transmission loss is shown in Fig. 9. Note the so-called Lloyd mirror pattern involving alternating bands of high and low intensity. These bands result from the alternating constructive and destructive interference between the source and its image reflected in the ocean surface. Again, the agreement between the FER and FFP is excellent throughout the domain.

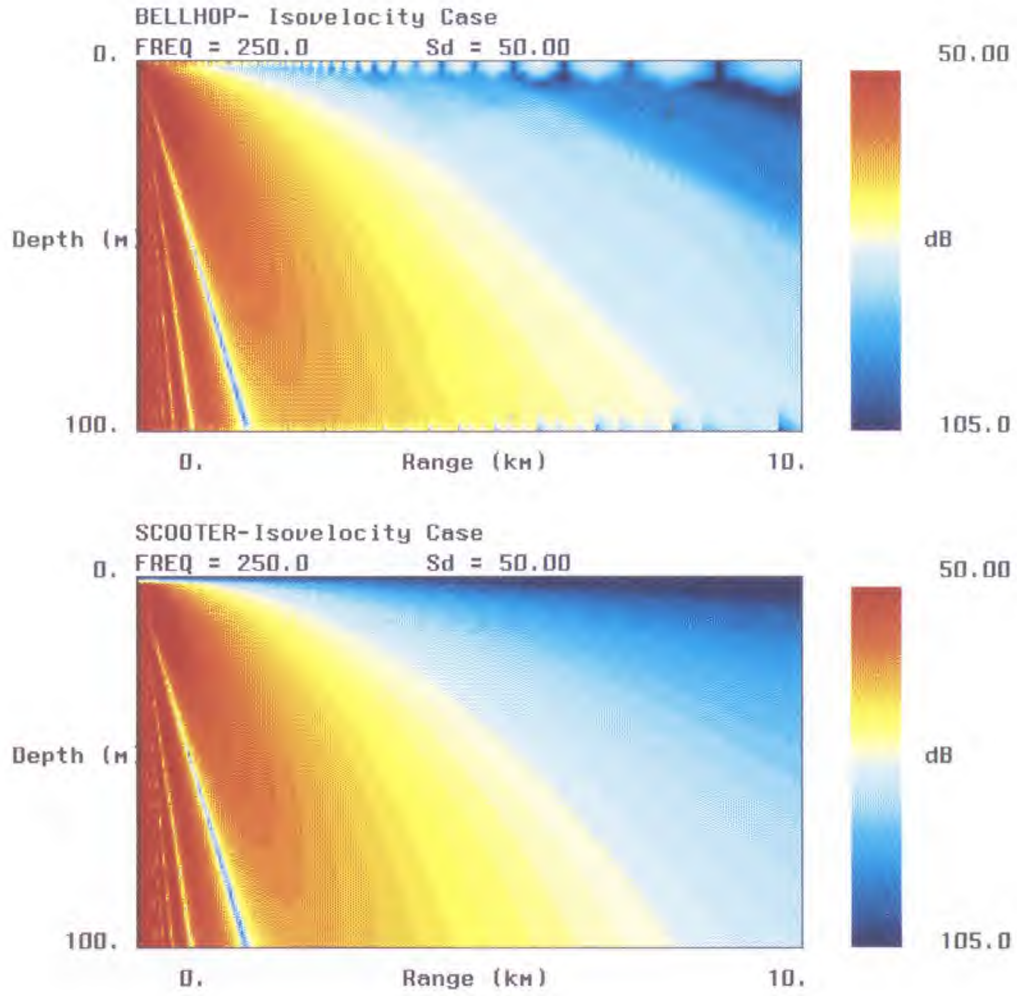

Figure 9: Transmission loss for the isovelocity case with a reflecting surface.

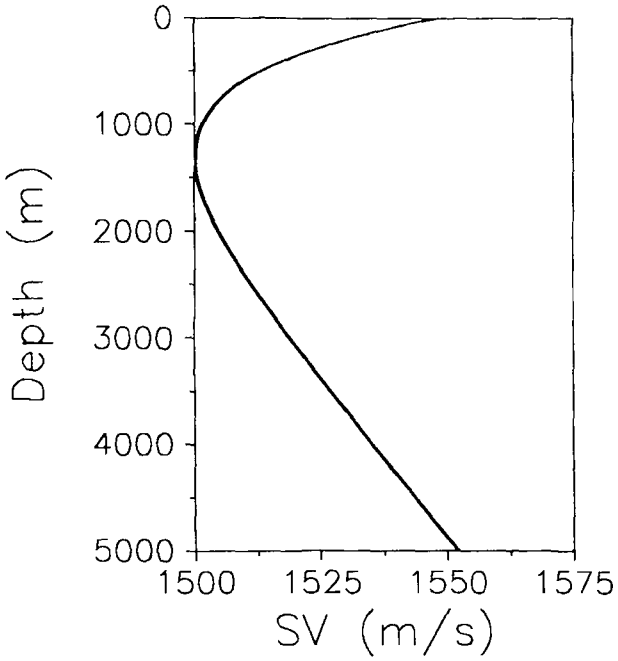

Figure 10: Sound speed plot for the munk profile

3.2 Munk Profile

In this next example we pass to a much more realistic case. This scenario involves deep water (5000 m) and a canonical sound speed profile (the Munk profile[11]) that is often used as a test problem. The sound speed for this profile is given by:

$$c(z) = 1500.0[1.0 + \varepsilon(z' - 1 + e^{-z'})]. \tag{59}$$

where

$$\varepsilon = 0.00737, \tag{60}$$

and the scaled depth z' is given by

$$z' = \frac{2(z - 1300)}{1300}. \tag{61}$$

This sound-speed profile is plotted in Fig. 10. The corresponding ray trace for a source at 1000 m depth is shown in Fig. 11. Notice that the rays form a cyclical pattern with a period of roughly 60 km. This is the so-called convergence-zone pattern which is typical of deep-water problems. We can also identify numerous caustics.

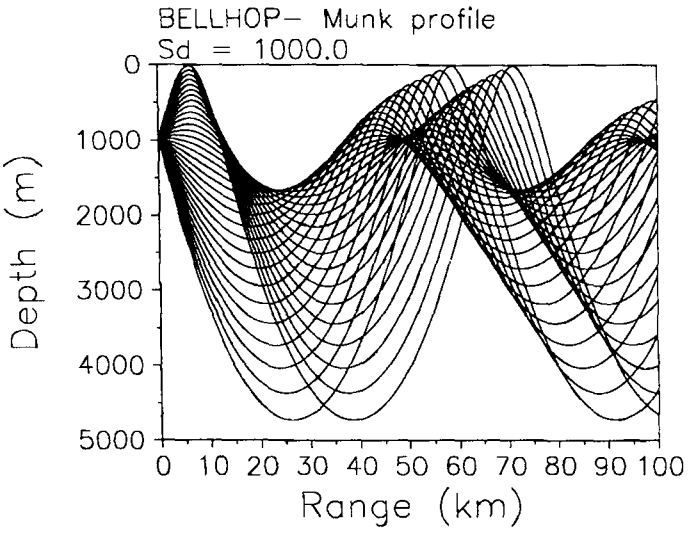

Figure 11: Ray trace for the munk profile

To simplify the picture we have suppressed bottom reflections. In this case, this is easily accomplished by restricting the ray fan to include only rays that are refracted before hitting the bottom. The upper surface is modeled as a vacuum. The resulting transmission loss field is shown in Fig. 12 for a source frequency of 50 Hz. Again we note the excellent agreement between the FER and FFP results. The caustics and foci of the ray trace are clearly visible in the FER result but these errors are confined to a small portion of the plot.

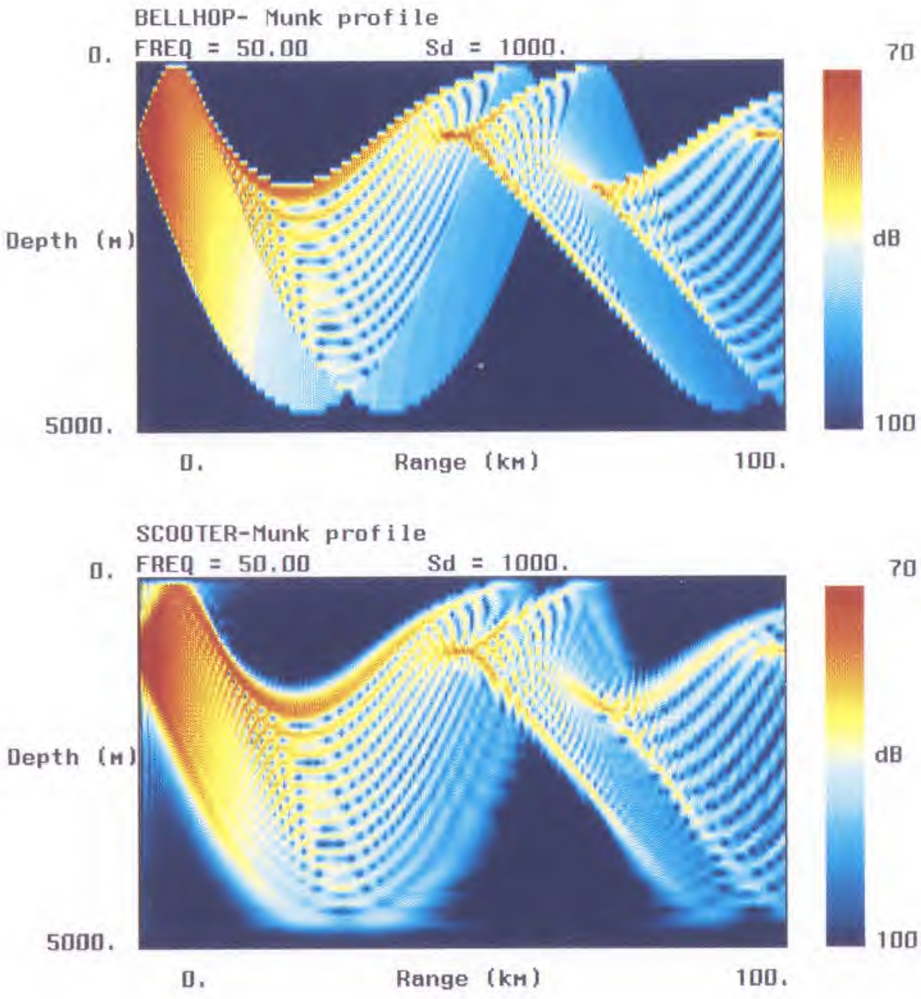

Figure 12: Transmission loss for the Munk profile.

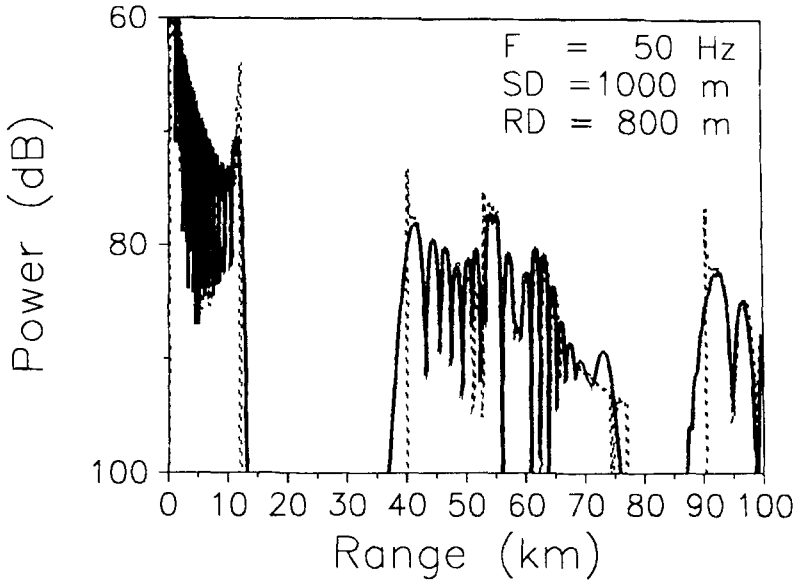

Figure 13: Transmission loss for the munk profile with half-space boundaries.

It is useful to look at a single slice to obtain a more quantitative measure of the agreement. In Fig. 13 we show a slice for a receiver depth of 800 m. Again we see excellent agreement apart from a few isolated zones where we pass near caustics of the ray field. Though the results are good in agreement, the cost of computation is remarkably different. The CPU time of the FER model is 18.5 s; meanwhile the CPU time of the FFP model is 188.05 s.

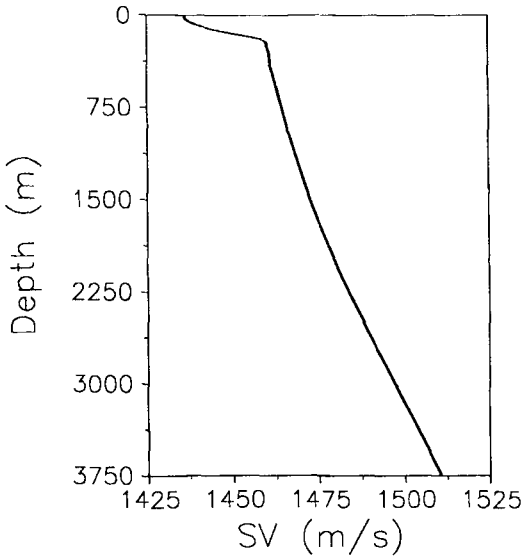

Figure 14: Sound speed for the arctic profile

3.3 Deep-water Arctic

Another important environment in underwater acoustics is the Arctic Ocean. Arctic profiles are typically upward refracting since there is no warming at the ocean surface to increase the sound speed. The particular case we consider is based on a measured sound speed profile obtained during the FRAM IV experiment. The sound speed profile (SSP) is plotted in Fig. 14. Here the bottom depth is 3750 m. The source frequency is taken to be 300 Hz and the source depth is 100 m.

Scattering by the rough ice canopy is a very complicated problem. It causes an effective loss due to scattering which can be included in our ray model. However, for the moment we will simply concentrate on the refractive effects of the medium and ignore the surface scattering.

In Fig. 15 we show the ray trace obtained for this problem with a source at a depth of 80 m. The corresponding transmission loss is shown in Fig. 16. Again we see the agreement is excellent throughout most of the region. In the near-field we see a Lloyd mirror pattern similar to the isovelocity case. However, here the refractive effects of the ocean medium distort the beams from straight line paths. We can also clearly

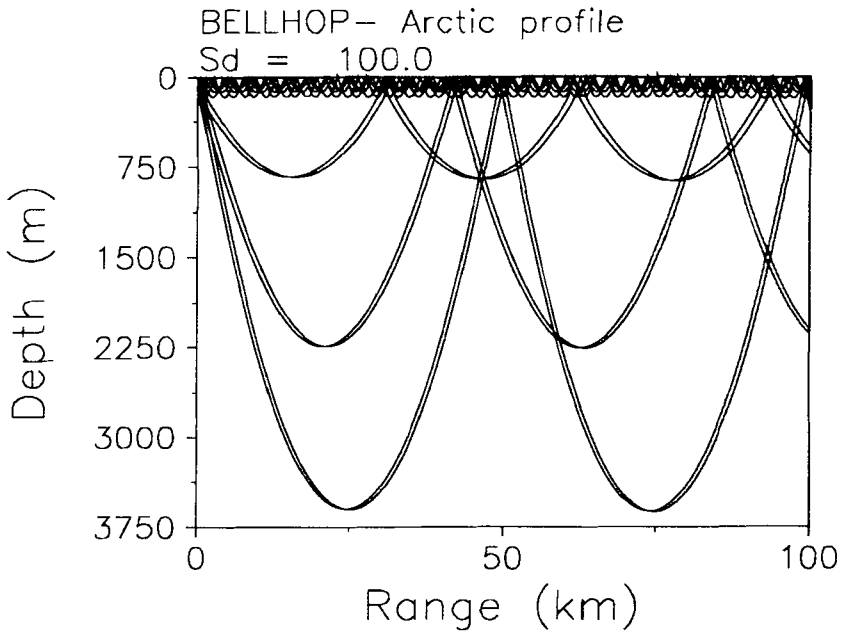

Figure 15: Ray trace for the arctic profile

see a band of energy trapped in the surface duct.

In Fig. 17 and Fig. 18 we examine two slice through the pressure field. The first is for a shallow receiver located in the surface duct at a depth of 100 m. The second is for a deep receiver located at a depth of 1000 m. The shallow receiver samples a much more complicated zone of the acoustic field. Rays in this region have a short loop length and numerous caustics. The overall field has a more complicated structure relative to that at a deeper depth. Primarily because of the large number of caustics, the agreement is worse for the shallow receiver than the deep receiver. However, the agreement is quite satisfactory in both cases.

The CPU time of the FER model is independent of frequency, however the CPU time of the FFP model increases very quickly as the frequency increases. For the 300 Hz frequency the CPU time of FER is 25.4 s, meanwhile, the CPU time of normal modes is 320.5 s.

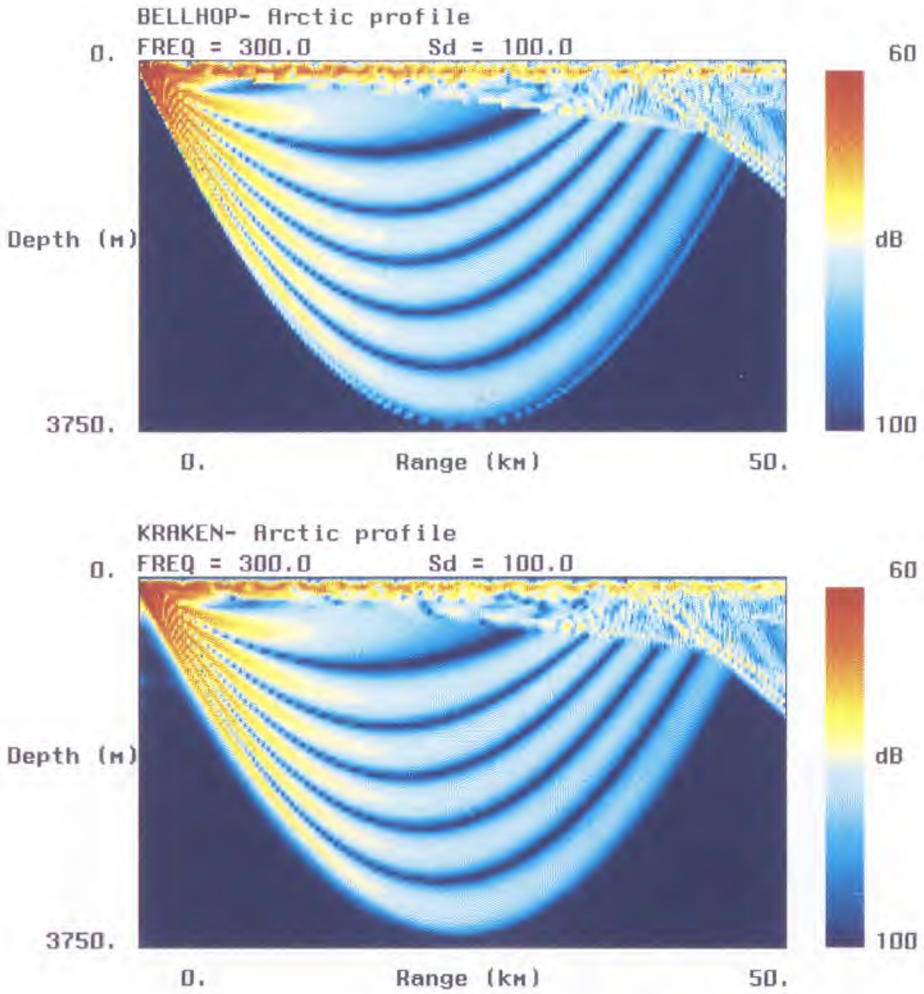

Figure 16: Transmission loss for the arctic profile.

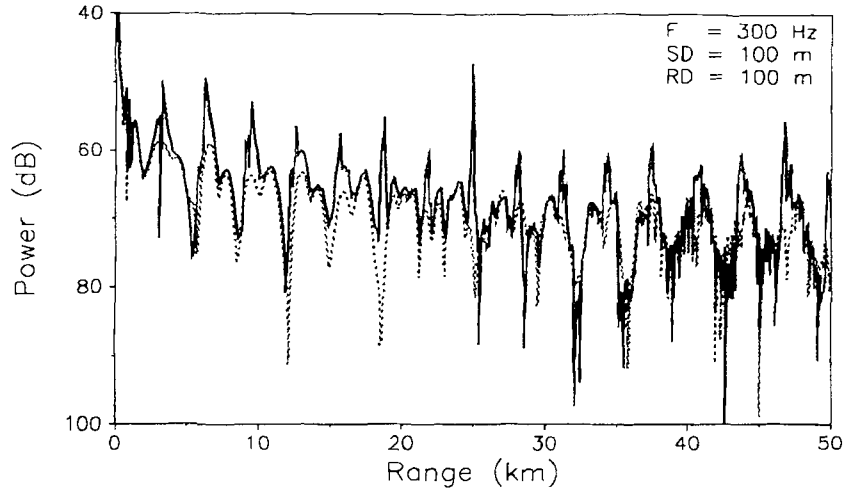

Figure 17: Transmission loss for the arctic profile.

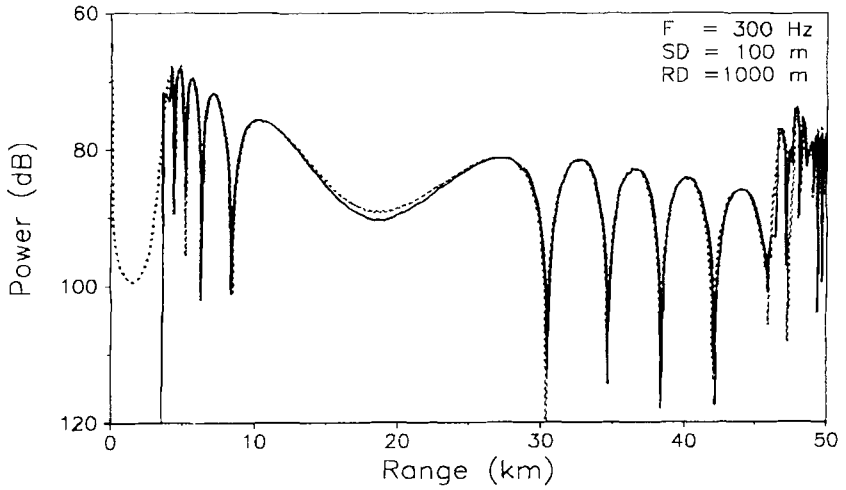

Figure 18: Transmission loss for the arctic profile.

3.4 Shallow-Water Case

The term 'shallow-water' is defined in different ways by different speakers. For the navy, shallow-water represents the coastal zone with depths less than a few hundred meters. Some individuals define shallow water in terms of the number of wavelengths in the water column. This sort of definition often makes sense in wave propagation problems. However, in underwater acoustics shallow water is characterized by numerous features that do not scale with frequency.

For instance, shallow water problems are often downward refracting due to the effects of surface heating. This changes the physics of the propagation in a dramatic way for then *all* paths are bottom reflected and the reflection coefficient of the ocean bottom becomes a critical factor.

To illustrate the performance of FER model in shallow water we will consider two cases. The environmental parameters for the two cases are illustrated in Fig. 19. The first of these cases is based on a well-known test problem from the NORDA PE workshop[5]. The parameters are all realistic except perhaps the sediment density. Early PE's were prone to difficulties in the case of large density jumps so the value was set artificially low. We will refer to this as the isovelocity shallow-water case.

The second case we shall consider modifies the first by introducing a gradient in the ocean medium. We shall refer to this as the gradient shallow-water case. Typically, shallow water problems vary from isovelocity to downward refracting. These two cases bracket the majority of such problems.

Turning now to the first (isovelocity) case we obtain the ray trace shown in Fig. 20 for a source depth of 50 m. A plot of the pressure field is provided in Fig. 21 where the source frequency is taken to be 250 Hz. The agreement is excellent. This may also be seen in Fig. 22 which shows a slice taken for a receiver depth of 50 m.

Recalling our previous results with an isovelocity case one might have expected such good results. However, it is important to remember that unlike the previous cases,

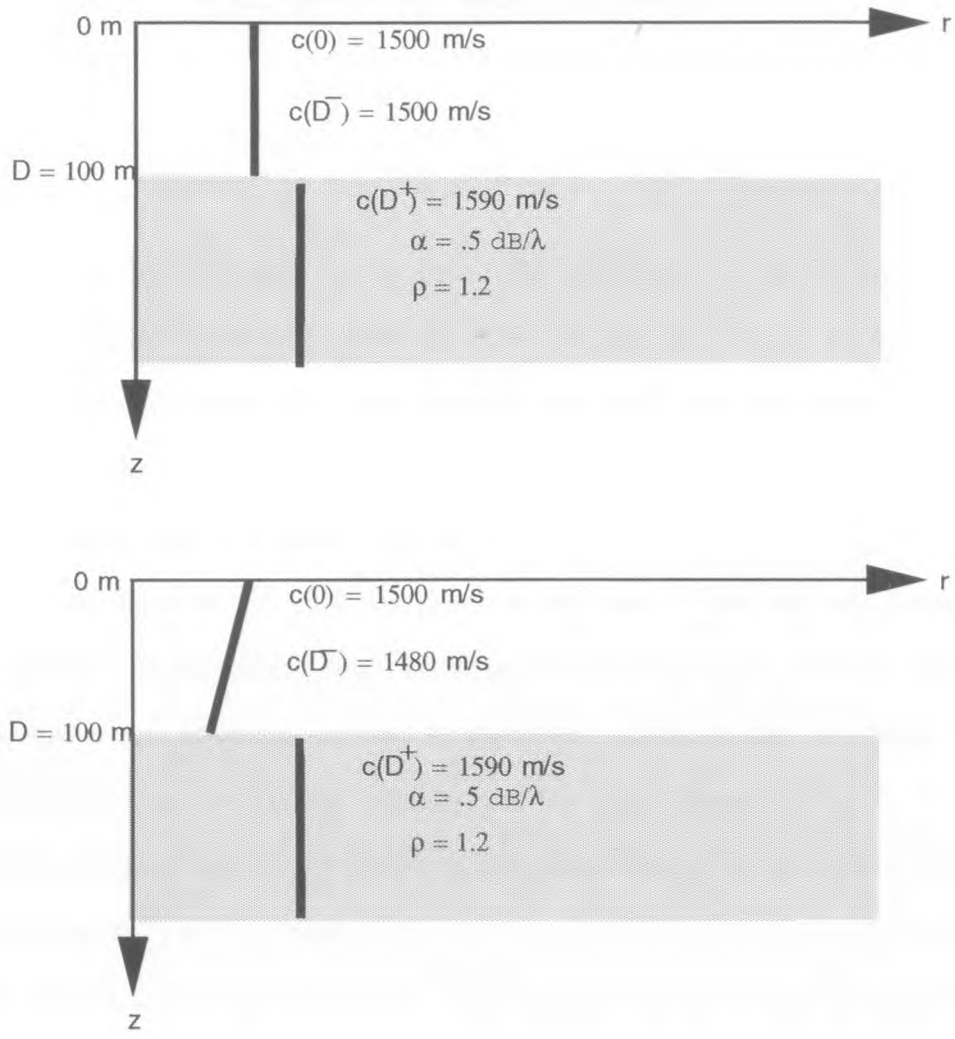

Figure 19: Schematics of the isovelocity and the gradient shallow-water case.

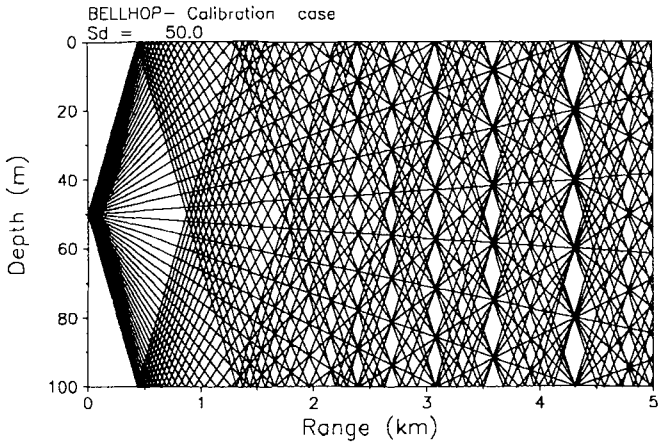

Figure 20: Ray trace for the isovelocity shallow-water case.

ray theory is *not* exact in this case. The difference is that we have included a half-space for the lower boundary. In effect we are considering a two-medium problem with one isovelocity layer over another. For such cases ray theory is not exact. The good agreement indicates that we have correctly treated the phase and amplitude of the surface and bottom reflections.

We now turn to the downward refracting case. The ray trace shown in Fig. 23 confirms the downward refracting nature of the gradient. Notice that the inclusion of this small gradient has had a significant effect on the ray trace. Of particular importance is that the ray picture now has many caustics.

These caustics are clearly visible in the transmission loss plot shown in Fig. 24. If we look carefully at the details of this plot we see that the agreement is excellent except in the vicinity of these caustics. This is easier to see in Fig. 25 where we have taken a slice for a receiver depth of 50 m. The spikes at a range of about 1.7 km and 3.3 km correspond to the location of the caustic.

The key point of interest about this case is that the gradient in a shallow water problem plays a key role in determining the accuracy of the FER model and ray theory

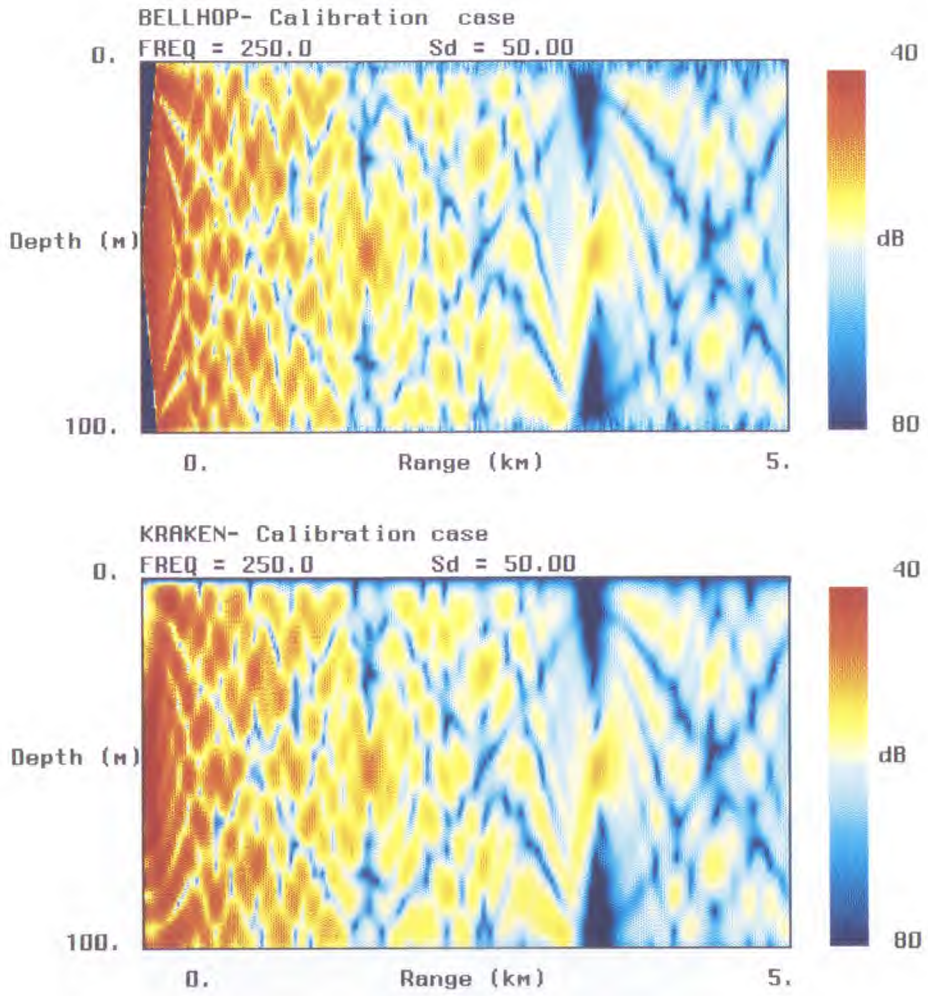

Figure 21: Transmission loss for the isovelocity shallow-water case.

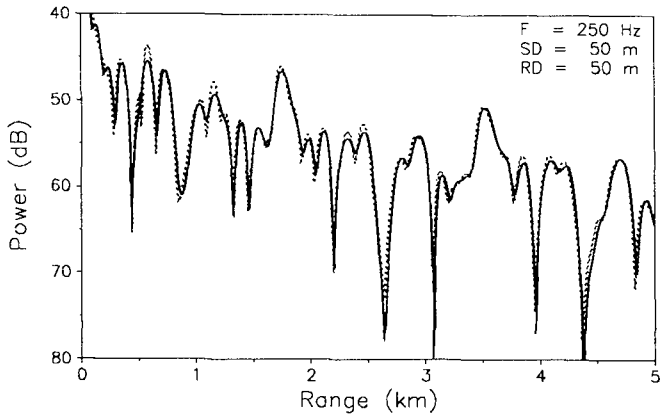

Figure 22: Transmission loss for the isovelocity shallow-water case.

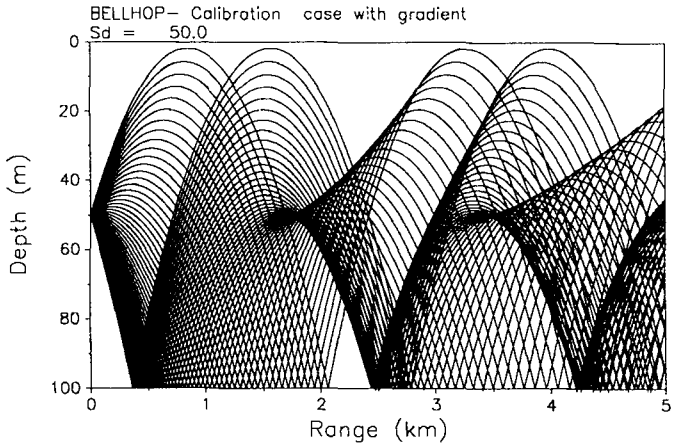

Figure 23: Ray trace for the gradient shallow-water case.

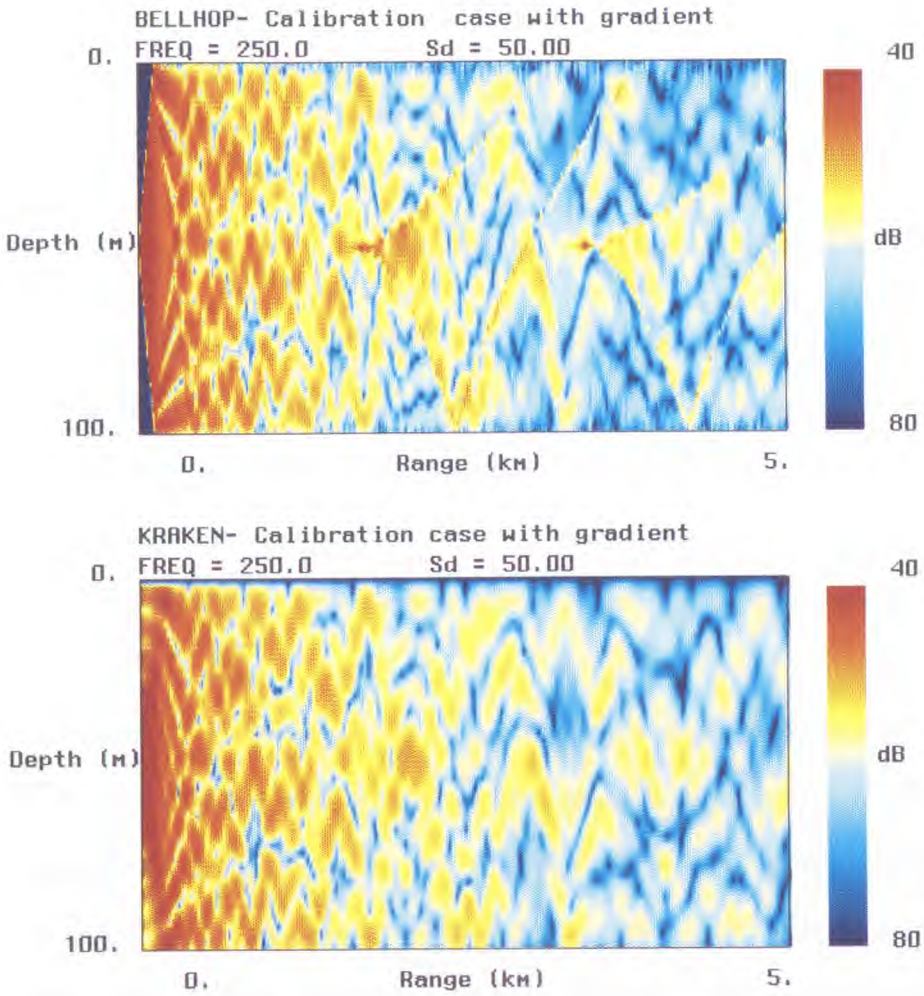

Figure 24: Transmission loss for the gradient shallow-water case .

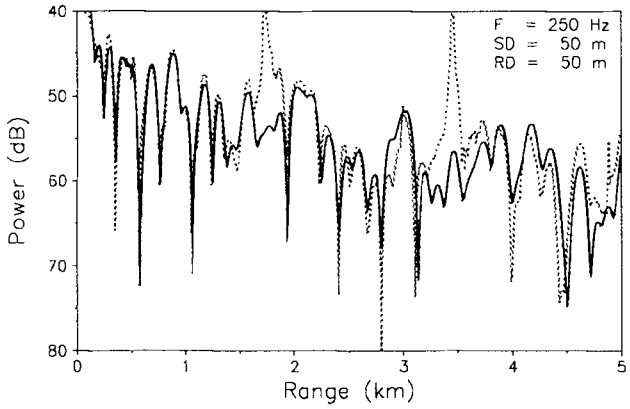

Figure 25: Transmission loss for the gradient shallow-water case.

in general. Frequently the question arises with ray theory as to how shallow the water depth can be (in wavelengths) before ray theory breaks down. This example shows that the answer depends not just on the depth of the channel; it is highly sensitive to the gradient since the gradient leads to the formation of caustics. Similarly, our judgement will depend on range since the density of caustics increases as we go out in range.

For the cases we have considered here the agreement is really quite acceptable in both cases. An interesting feature of this problem is that all ray paths are bottom interacting. In the far-field the contributing paths involve many bottom reflections. Thus, any error in the treatment of bottom reflections tends to accumulate in the far-field. The excellent agreement with the reference solution indicates that the FER model is treating the reflection properly at the interface of different media.

CHAPTER 4

CONCLUSIONS AND SUGGESTION

Ray tracing is based on high-frequency asymptotics and is therefore an approximate method. Nevertheless, ray methods are still widely used since they are much more rapid than the alternatives for high-frequency or broad band problems. Unfortunately, ray models can be difficult to implement and generally show serious flaws beyond those that are implicit in the mathematical derivation. As such, most ray models are unable to actually produce a true ray theory result and ray theory has a much poorer reputation for accuracy than it deserves.

The problem is to provide an algorithm to efficiently implement ray theory without introducing additional numerical artifacts. The FER formulation that we have described eliminates problems with 'drop-outs' that occur in other ray models when they fail to locate an eigen-ray connecting the source and receiver. The method borrows ideas from Gaussian beam tracing to completely eliminate the eigen- ray finding procedure. This will be especially important in 3D models.

Compared to Gaussian beam tracing the FER approach has both positive and negative aspects. Gaussian beams are free of caustics and shadow zones. The FER approach may still manifest these artifacts. On the other hand, there are no free parameters in this FER formulation. The selection of the free parameters in the Gaussian beam method has been an obstacle to the wide-acceptance of that approach. The various test cases that we have considered all show excellent agreement between the FER approach and more computationally intensive full-wave theories. It should be emphasized that these highly-accurate results are not typical of other production of ray models.

Other popular methods, such as the FFP and normal modes, are much more computationally intensive than the standard ray tracing method. Thus, for some cases, the

ray method continues to be attractive. Sometimes there is no practical alternative. There are still many interesting issues to address with this approach. Of key interest will be the extension to three-dimensional problems. This sort of a tool will be very useful for tomography and global acoustic thermometry research.

In terms of the simpler 2D case the remaining issues are to include a more complicated multi-layer model of the sediment and to address the importance of beam displacement. Tindle[18] has suggested that a significant improvement in conventional ray theory may be obtained by including this beam displacement.

REFERENCES

[1] Batorsky, D.V. and L.B. Felsen, 1971. *Ray optical calculation of model excited by sources and scatterers in weakly inhomogeneous duct*, Radio Sci. 6, 911-923.

[2] Bleistein, N. 1984. *Mathematical methods for Wave Phenomenon*. Freeman, New York

[3] Červený, V., M.M. Popov and I. Pšenčík, 1982. *Computation of wave fields in inhomogeneous media — Gaussian beam approach* , Geophys. J. R. Astr. Soc. 70, 109–128.

[4] Červený, V. and I. Psencik, 1984. Gaussian beams in elastic 2-D laterally varing layered structures, Geophys. J.R. Astron. Soc. 78, 65-91.

[5] Davis,J.A., D. White, and R.C. Cavanagh, 1982. *NORDA parabolic equation workshop*, Rep. TN-143 (Naval Ocean Research and Development Activity, Stennis Space Center, MS).

[6] Foreman,T.L., 1983. *Ray modeling methods for range dependent ocean environments*, Rep. TR-83-41 (Applied Research Laboratories, Austin, TX).

[7] Jensen, F. and W. Kuperman, M. Porter and H. Schmidt, 1994. *Computational Ocean Acoustics*. *American Institute of Physics*. New York.

[8] Keller, J.B., 1978. *Rays, waves and asymptotics*. Bull. Amer. Math. Soc. 84, 727-750.

[9] McGirr, R.W., D.B. King, J.A. Davis, J. Campbell, 1985. *An evaluation of range-dependent ray theory models*. NORDA Report 115.

[10] Moler, C.B. and L.P. Solomon, 1970. *Use of splines and numerical integration in geometrical acoustics*, J. Acoust. Soc. Am. 48, 739–744.

[11] Munk, W.H., 1974. *Sound channel in an exponentially stratified ocean with applications ti SOFAR*, J. Acoust. Soc. Am. 55, 224-252.

[12] Pedersen, M.A., 1961. *Acoustic intensity anomalies introduced by constant velocity gradients*, J. Acoust. Soc. Am. 31, 465–474.

[13] Porter, M.B. and Homer P. Bucker, 1987. *Gaussian beam tracing for computing ocean acoustic fields*, J. Acoust. Soc. Am. 82(4), 1349-1359.

[14] Porter, M.B., 1991. *The KRAKEN normal mode program*, SACLANTCEN Memorandum. no: SM-245.

[15] Roberts, B.G. 1974. *Horizontal-gradient acoustical ray-trace program TRIMAIN*, Rep. 7827 (Naval Research Laboratory, Washington, DC).

[16] Thompson, P.A., 1972. *Compressible-fluid dynamics*, McGRAW-Hill Book Company.

[17] Tindle, C.T. and G.E.J. Bold, 1981. *Improved ray calculations in shallow water*, J. Acoust. Soc. Am. 70, 813–819.

[18] Tindle, C.T. 1983. *Ray calculation with beam displacement*, J. Acoust. Soc. Am. 73(5), 1581-1586.

[19] Cornyn J. J., 1973 *GRASS: A digital-computer ray-tracing and transmission-loss-prediction system*, Rep. 7621 (Naval Research Laboratory, Washington, DC).

[20] Watson, W.H. and R. McGirr, 1975. *RAYWAVE II: A propagation loss model for the analysis of complex ocean environments*, Rep. TN-1516 (Naval Ocean Systems Center, San Diego, CA).

[21] Westwood, E.K. and P.J. Vidmar, 1987. *Eigenray finding and time series simulation in a layered bottom*, J. Acoust. Soc. Am. 81, 912–924.